Journal of Petroleum Science and Engineering 129 (2015) 48–57

Contents lists available at ScienceDirect

Journal of Petroleum Science and Engineering

journal homepage: www.elsevier.com/locate/petrol

Pore-scale analysis of formation damage in Bentheimer sandstone with in-situ NMR and micro-computed tomography experiments

Ahmed Z. Al-Yaseri [a], Maxim Lebedev [b], Sarah J. Vogt [c], Michael L. Johns [c], Ahmed Barifcani [d], Stefan Iglauer [a,*]

[a] Curtin University, Department of Petroleum Engineering, 26 Dick Perry Avenue, Kensington, WA 6151, Australia
[b] Curtin University, Department of Exploration Geophysics, 26 Dick Perry Avenue, Kensington, WA 6151, Australia
[c] University of Western Australia, School of Mechanical and Chemical Engineering, 35 Stirling Highway, Crawley, WA 6009, Australia
[d] Curtin University, Department of Chemical Engineering, 26 Dick Perry Avenue, Kensington, WA 6151, Australia

ARTICLE INFO

Article history:
Received 10 October 2014
Accepted 9 January 2015
Available online 19 January 2015

Keywords:
Formation damage
Micro tomography
NMR
Plugging mechanism
Permeability reduction

ABSTRACT

We investigated fines movement through sandstone in-situ at the micrometre pore scale and studied the associated pore-scale mechanisms leading to formation damage. We used two in-situ techniques to accomplish this, namely nuclear magnetic resonance T_2 relaxation time (NMR) measurements (of pore size distributions) and high resolution x-ray micro-computed tomography (μCT; at high resolutions of $(0.89\ \mu m)^3$ and $(3.4\ \mu m)^3$). The μCT images showed the precise 3D location of the fines particles in the plug and demonstrated that initially pore throats are plugged, followed by filling of adjacent pore bodies by solid particles. These measurements in combination with traditionally used (indirect) permeability and production curve measurements and ex-situ SEM imaging enabled us to propose a new mechanistic pore-scale plugging model; furthermore we demonstrated that the amount of fines trapped decayed rapidly with core depth. We conclude that it is feasible to analyse formation damage in-situ by a combination of NMR and μCT measurements.

1. Introduction

Migration of colloids ($\leq 5\ \mu m$) and dispersed small solid particles ($< 100\ \mu m$) through a porous medium is a key problem in various fields as deposition of such particles can severely reduce permeability. Areas which face this problem include hydrology, where the focus is on water production (McDowell-Boyer et al., 1986; Bradford et al., 2011; Torkzaban et al., 2007), geothermal engineering, where cold water is pumped through subsurface reservoirs to produce warm water (Mahmoudi et al., 2010; Rosenbrand et al., 2014, 2015), wellbore drilling (Byrne et al., 2007; Civan, 2007) and petroleum recovery, where water is injected to maintain reservoir pressure and mobilize additional hydrocarbons by viscous forces (Ahmed and McKinney, 2005; Iglauer et al., 2010).

Common to all these processes is that water added to a reservoir can cause the release of colloids and fine particles in the rock due to subtle changes in fluid composition (Ryan and Elimelech, 1996) or through shear forces (Tran et al., 2009); furthermore, surface water – which freely percolates into the formation due to gravitational forces or may be injected by force in an industrial process – contains fine particles (McDowell-Boyer et al., 1986; Bennion et al., 2011) as filtration is uneconomical (Bennion et al., 2011). Consequently, in case of injected water, certain quality requirements need to be fulfilled, i.e. the water must not contain solid particles which are larger than a certain maximum size (Bennion et al., 1998). It is thus important to understand the particles' impact on fluid dynamics and associated pore-scale plugging mechanisms, which cause the formation damage (Nowak and Krueger, 1951; Krueger, 1967; McDowell-Boyer et al., 1986; Ryan and Elimelech, 1996; Civan, 2007; Rosenbrand et al., 2014,2015).

Traditionally, various techniques were used to investigate the characteristics of such formation damage. This usually included the measurement of the injection flow rate and pressure drop across the sample to determine dynamic permeability, and the measurement of produced fluid mass versus time (e.g. Krilov et al., 1991; Asghari et al., 1995; Tran et al., 2010). Frequently these measurements were supported by x-ray diffraction (XRD) measurements (e.g. Krilov et al., 1991; Seright et al., 2006; Potter et al., 2011; Green et al., 2013) and petrographic thin section analysis (e.g. Gulati and Maly, 1975; Bowers et al., 1995; Hidajat et al., 2002;

* Corresponding author.
E-mail addresses: a.al-yaseri@postgrad.curtin.edu.au (A.Z. Al-Yaseri), m.lebedev@exchange.curtin.edu.au (M. Lebedev), sarah.vogt@uwa.edu.au (S.J. Vogt), michael.johns@uwa.edu.au (M.L. Johns), a.barifcani@curtin.edu.au (A. Barifcani), stefan.iglauer@curtin.edu.au (S. Iglauer).

http://dx.doi.org/10.1016/j.petrol.2015.01.018
0920-4105/

Green et al., 2013). Furthermore scanning electron microscopy (SEM) was used to study fines deposition at the nanometre to micrometre scale (e.g. Kandarpa and Sparrow, 1981; Byrne et al., 2000; Green et al., 2013), and nuclear magnetic resonance (NMR) T_2 relaxation measurements were used to probe changes in the associated pore size distributions (Tran et al., 2010; Fischer et al., 2011). More recently, medical x-ray computer tomography has been used to image the distribution of fines within the rock at low spatial resolution (1 mm) (Tran et al., 2010; Green et al., 2013).

However, all these techniques have serious limitations: dynamic permeability measurements and fluid mass production curves are indirect observations, while thin section analysis, XRD and SEM only measure ex-situ data. NMR is a bulk measurement and does not provide information about spatial distributions. 3D medical x-ray tomography, however, can provide a 3D spatial map of the CT numbers (which is related to the x-ray attenuation of the different minerals (Okabe et al., 2013)), but here spatial resolution is low (0.5–1 mm) and individual pores or fine particles can thus not be observed.

Recently, with the advent of micro-computed tomography (μCT), it has become possible to overcome these limitations (Blunt et al., 2013; Wildenschild and Sheppard, 2013). Green et al. (2013) for instance imaged representative core samples of varying permeabilities (8 to 7000 mD) at a μCT resolution of 10–15 μm in-situ in order to investigate the damage caused by drilling mud invasion.

We are now paying attention to the detailed pore-scale plugging mechanisms via a combination of high resolution μCT imaging (0.9 μm and 3.4 μm resolution), standard coreflooding, SEM and NMR analysis. Using these methods we were able to visualize the precise 3D distribution of fines within the pore space of the plug, and were able to develop a new mechanistic plugging model; we discuss this new model in the context of established literature models.

2. Experimental methodology

2.1. Materials

The experiments were performed on two homogeneous cylindrical Bentheimer sandstone plugs (diameter = 5.2 mm, length = 32.5 mm); these were sister plugs drilled from the same block, the drill holes were just adjacent to each other. Their brine permeabilities were 559 mD and 523 mD, and their porosities were 21% and 23%, Table 1. The composition of the Bentheimer sandstone was measured via XRD with a Bruker-AXS D9 Advance Diffractometer (Kaolinite 0.7 wt%, Quartz 99.0 wt%, Rutile 0.3 wt%) on a fragment obtained from the same block just adjacent to the drill holes; this indicated that the sandstone was quite clean and consisted mainly of quartz.

As a representative for the fines in the subsurface, we selected a fine barite powder (Krilov et al., 1991; Tran et al., 2010). The barite

Table 1
Bentheimer sandstone porosities and permeabilities before and after fines injection.

	Porosity measured by μCT	Porosity measured by NMR	Brine permeability (Darcy)
Sample #1 before damage	0.21	0.21[a]	0.559
Sample #2 before damage	0.23	0.23[a]	0.523
Sample #1 damage by 10 g/L barite	0.15	0.176	0.11
Sample #2 damage by 20 g/L barite	0.10	0.121	0.048

[a] The initial porosity was set to the μCT porosity, see left column.

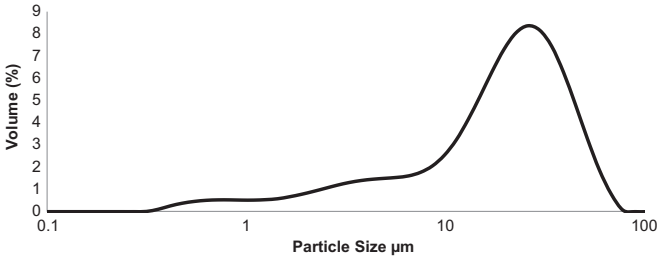

Fig. 1. Particle size distribution of barite powder used in the experiments.

particles had a broad particle size distribution, which ranged from 0.4 to 80 μm and peaked at 25 μm, Fig. 1 (measured with a Mastersizer Malvern Hydro 2000S). The barite particles were suspended in brine (5 wt% NaCl + 1 wt% KCl in deionized water) by constant agitation with a magnetic stirrer.

2.2. Simulation of fines migration in the subsurface

In order to mimic fines flow in the subsurface, the Bentheimer plugs were sealed with a PTFE heat shrink sleeve, which was cured at 653 K for ~20 min, vacuumed for 40 min, and then saturated with brine. Subsequently the brine permeability of each plug was measured by injecting water at a constant flow rate with a peristaltic pump (Masterflex model 7518-10), while the pressure drop across the plug was measured; brine permeability was then calculated using Darcy's law. This permeability measurement was continued during fines injection, see below. The samples were then imaged with a μCT scanner (Xradia Versa XRM-500T) at a resolution of $(3.4\ \mu m)^3$, and NMR T_2 response curves were measured for each specimen on a (^{1}H resonance) 20 MHz Bruker Minispec benchtop NMR instrument. The NMR T_2 response time correlates with the pore size distribution in the core (Talabi et al., 2009; Fridjonsson et al., 2013), and it thus constitutes an independent measurement.

The samples were then flooded with the barite suspension (two different barite concentrations were tested: 10 g/L and 20 g/L), and simultaneously the mass of produced fluid was measured with a balance (Phoenix, BTA/BTB series, accuracy = 0.001 g) as a function of time. All experiments were conducted at ambient conditions, i.e. 130,000 Pa (± 20,000 Pa) pressure and (296 K ± 2 K) temperature.

Once the plug samples were highly damaged by the fines injection process (permeability reduced by ~90%), the plugs were μCT imaged again at two different but high resolutions $(3.4\ \mu m)^3$ and $(0.89\ \mu m)^3$. All μCT images were filtered with a non-local means filter (Buades et al., 2005) and segmented according to Otsu's algorithm (Otsu, 1979). On the segmented images porosities, pore volumes, and pore radius distributions were measured; we note that these parameters are affected by fines migration (Civan, 2007). Furthermore, the precise 3D location of the barite particles was observed, this is discussed further below.

After μCT scanning the plugs were subjected to another NMR T_2 response measurement to measure any changes in the pore size distributions.

3. Result and discussion

The evolution of the permeability with time during fines suspension injection is shown in Fig. 2. The permeability (k) continuously and smoothly decreased with time (t) following a power law $k = 3.94t^{-0.343}$, Pearson coefficient $R^2 = 0.996$, (sample#1); $k = 2.701t^{-0.403}$, $R^2 = 0.978$ (sample#2), and the permeability reduction was more significant for the higher barite concentration as expected, consistent with trends reported in the literature (Krilov et al., 1991; Asghari et al., 1995);

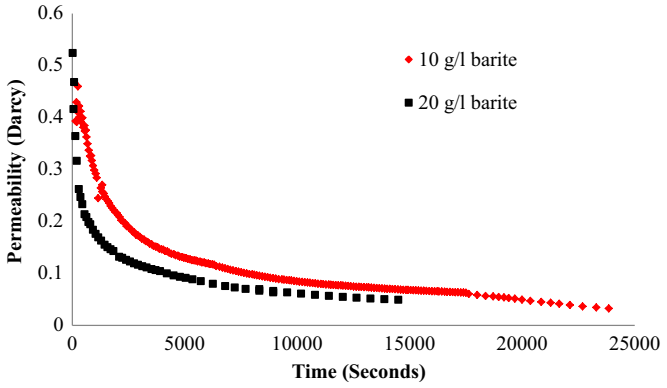

Fig. 2. Permeability measured versus time for different barite concentrations (10 g/L and 20 g/L). The permeability (k) continuously and smoothly decreased with time (t) following a power law, $k=3.94t^{-0.343}$, $R^2=0.996$ for 10 g/L); and $k=2.701t^{-0.403}$, $R^2=0.978$ for 20 g/L.

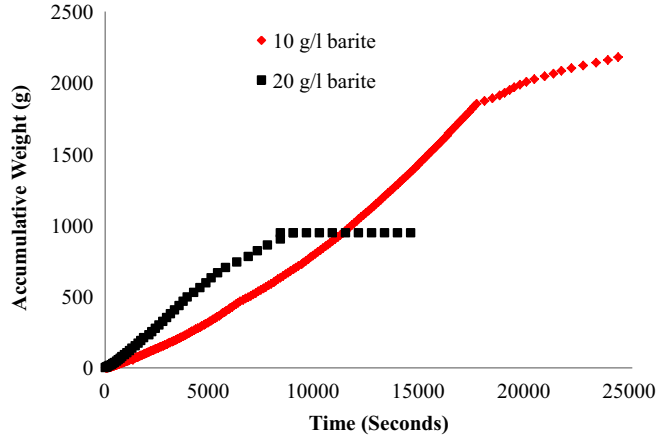

Fig. 3. Accumulative weight of produced fluid versus time for different barite concentrations (10 g/L and 20 g/L).

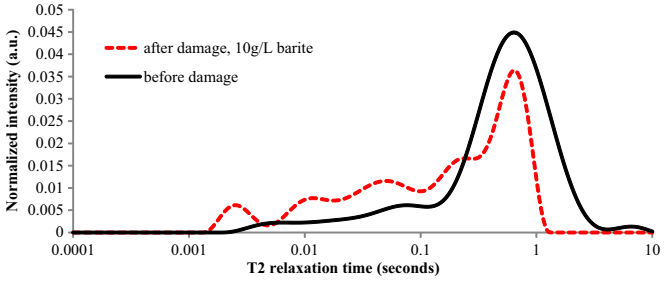

Fig. 4. NMR T_2 response curves before and after injection of 10 g/L barite suspension. Porosity was reduced from 21% to 17.6%.

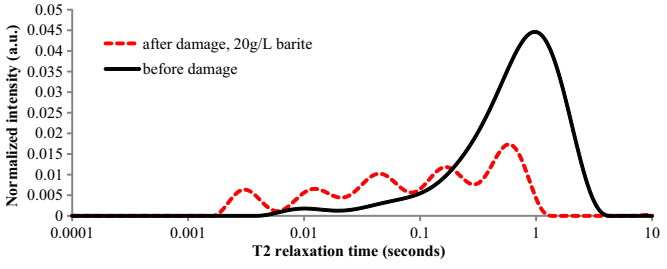

Fig. 5. NMR T_2 response curves before and after injection of 20 g/L barite suspension. Porosity was reduced from 23% to 12.1%.

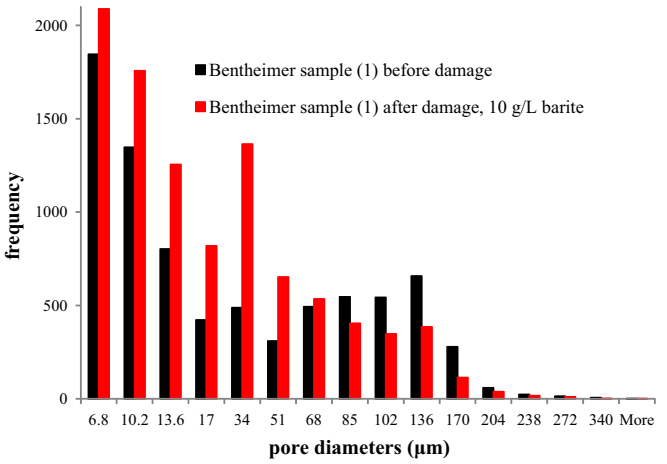

Fig. 6. Bentheimer #1 pore diameters before and after damage caused by fines injection (10 g/L barite) measured with μCT.

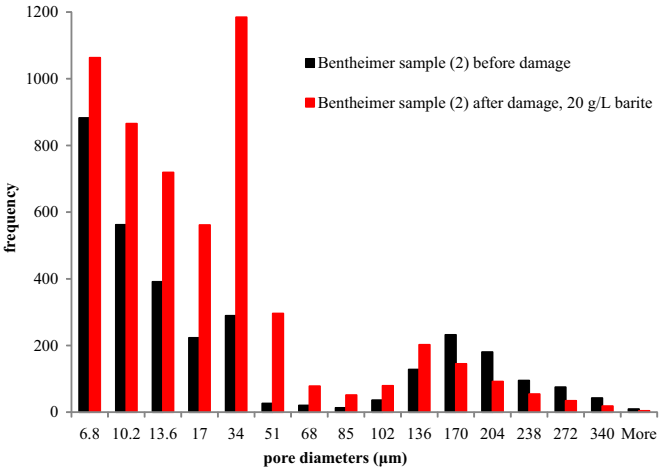

Fig. 7. Bentheimer #2 pore diameters before and after damage caused by fines injection (20 g/L barite) measured with μCT.

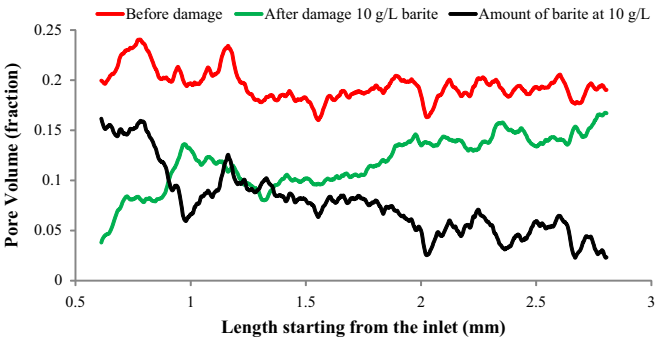

Fig. 8. Porosity versus core length before (red) and after (green) damage and amount of barite trapped (black) versus core depth (10 g/L barite). (For interpretation of the references to colour in this figure legend, the reader is referred to the web version of this article.)

moreover, Nguyen and Civan (2005) and Tran et al. (2009 and 2010) observed an exponential correlation for the dynamic permeability as a function of time with exponents and coefficients depending on several variables including α (cement exclusion parameter, dimensionless), σ (particle volume fraction, fraction), and β (pore-to-particle diameter, dimensionless), which is approximately consistent with our results. Specifically, we measured a permeability reduction from 559 mD to

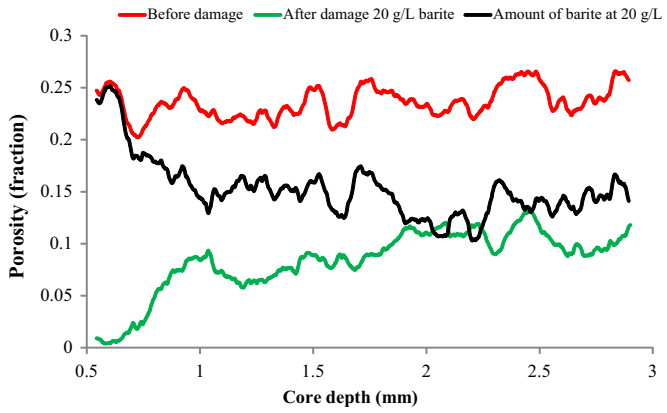

Fig. 9. Porosity versus core length before (red) and after (green) damage and amount of barite trapped (black) versus core depth (20 g/L barite). (For interpretation of the references to colour in this figure legend, the reader is referred to the web version of this article.)

110 mD for 10 g/L barite concentration and from 523 mD to 48 mD for 20 g/L barite concentration. The plugging time (note that plugging occurs at the discontinuity in the production curve (Tran et al., 2009, 2010), Fig. 3) was faster when the particles' concentration increased. Plugging time was 1.38 h for the 20 g/L suspension, while it was 4.47 h for the 10 g/L suspension, Fig. 3.

Note that plugging time for Krilov et al. (1991)'s study was ≈30 min, they flooded outcrop sandstone (permeabilities 144, 1549, 71, 40 mD and porosities 13.3, 21.2, 22.7 and 21.2 respectively) with barite suspensions (particle sizes varied from 2 to 60 μm); Asghari et al. (1995) reported plugging times ≈200 min after injecting filtered sea water (filtration through a 10 μm filter) through carbonate rock (core plugs from Siri oil field in Iran with an average permeability of 7.9 mD and average porosity 20%); and Tran et al. (2010) reported a plugging time ≈2.5 h after injecting drilling mud (bentonite and barite with 5 wt% barite concentration and 1.2 to 12 μm barite particles size range) through Berea sandstone samples (permeabilities 1240, 265 mD and porosity 20.6%, 17.5%, respectively).

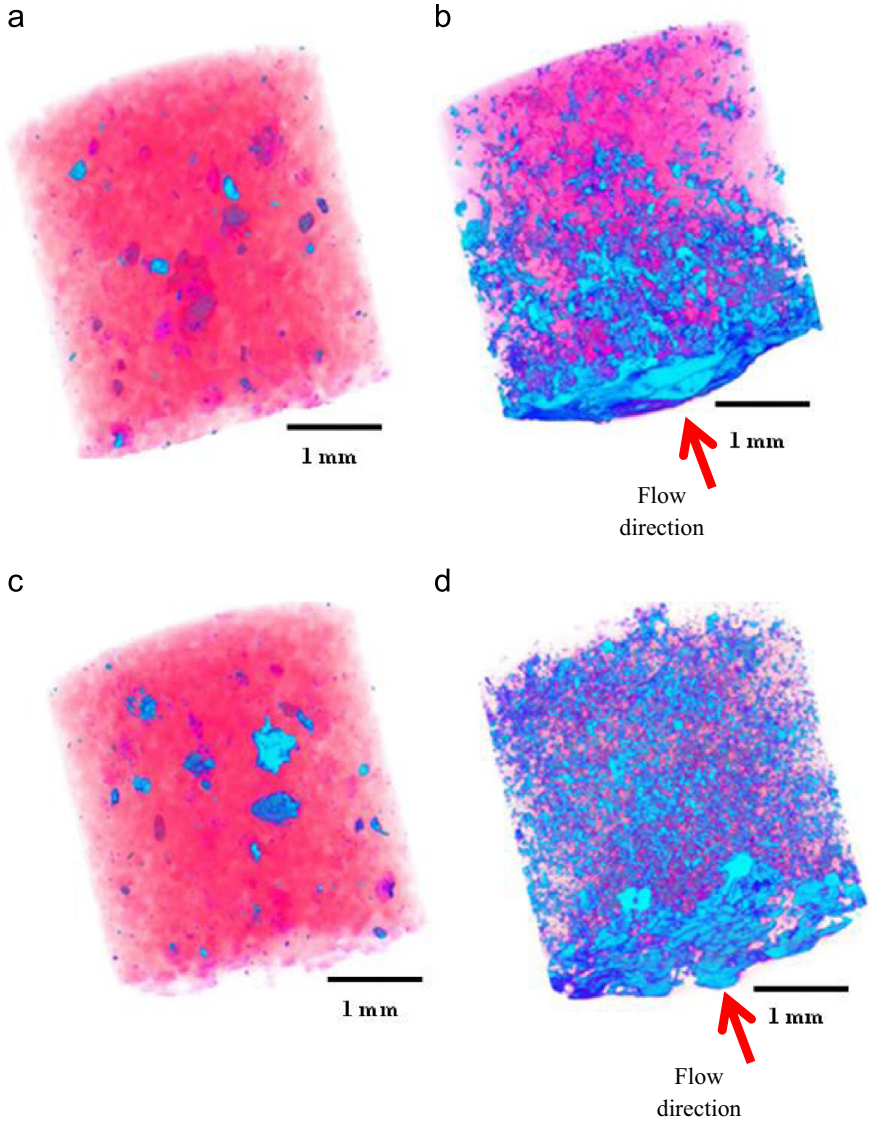

Fig. 10. 3D μCT images (3.4 μm resolution) of the core plugs before and after barite injection; (a) is sample #1 and (c) is sample #2 before damage, (b) is sample #1 after damage (10 g/L barite) and (d) is sample #2 after damage (20 g/L barite). The cylindrical volumes shown are 3.4 mm in diameter and 3.4 mm in length (=30.86 mm^3). In the images (a) and (c) rutile (component of original rock, see XRD analysis above) is blue and sandstone (quartz) is pink. In the images (b) and (d) the deposited barite is also blue. (For interpretation of the references to colour in this figure legend, the reader is referred to the web version of this article.)

Figs. 4 and 5 show the NMR T_2 response curves for the undamaged and damaged samples for both fines concentrations, respectively. The T_2 NMR measurement is related to the surface S to volume V ratio of the pore structure by the equation $1/T_2 = \rho S/V$, where ρ is the surface relaxivity, a parameter dependent on the composition of the rock (Kleinberg et al., 1994), which we assume to be constant between the two Bentheimer samples tested in this work. Therefore, a shorter T_2 relaxation time corresponds to a larger surface to volume ratio and thus smaller pores. Initially the NMR signal indicated a primarily homogeneous pore space, with approximately 10–20% of the signal originating from secondary (smaller) pores, consistent with previous measurements for similar sandstone (Liaw et al., 1996). The integral of the NMR T_2 signal, which corresponds to the amount of water in the pore space, was substantially reduced for the damaged samples, which corresponds to a substantially reduced porosity (Allen et al., 1997), Table 1. This was measured for both fines concentrations, although the 20 g/L suspension was more effective in terms of porosity reduction. Furthermore, the bimodal character of the pore space changed into a multimodal system indicating that the homogeneous larger pores were segmented into heterogeneous smaller pores after damage (Liaw et al., 1996). Moreover, the average T_2 times for the samples calculated from the distributions in Figs. 4 and 5 decreased after the samples were damaged with barite indicating smaller pores sizes. The average T_2 time of the sample injected with 10 g/L barite suspension decreased from 0.72 s before damage to 0.31 s after damage, a reduction of 57%. For the sample injected with 20 g/L barite suspension, the average T_2 time decreased from 0.86 s to 0.25 s, a reduction of 71%. This clear shift in the NMR T_2 response towards

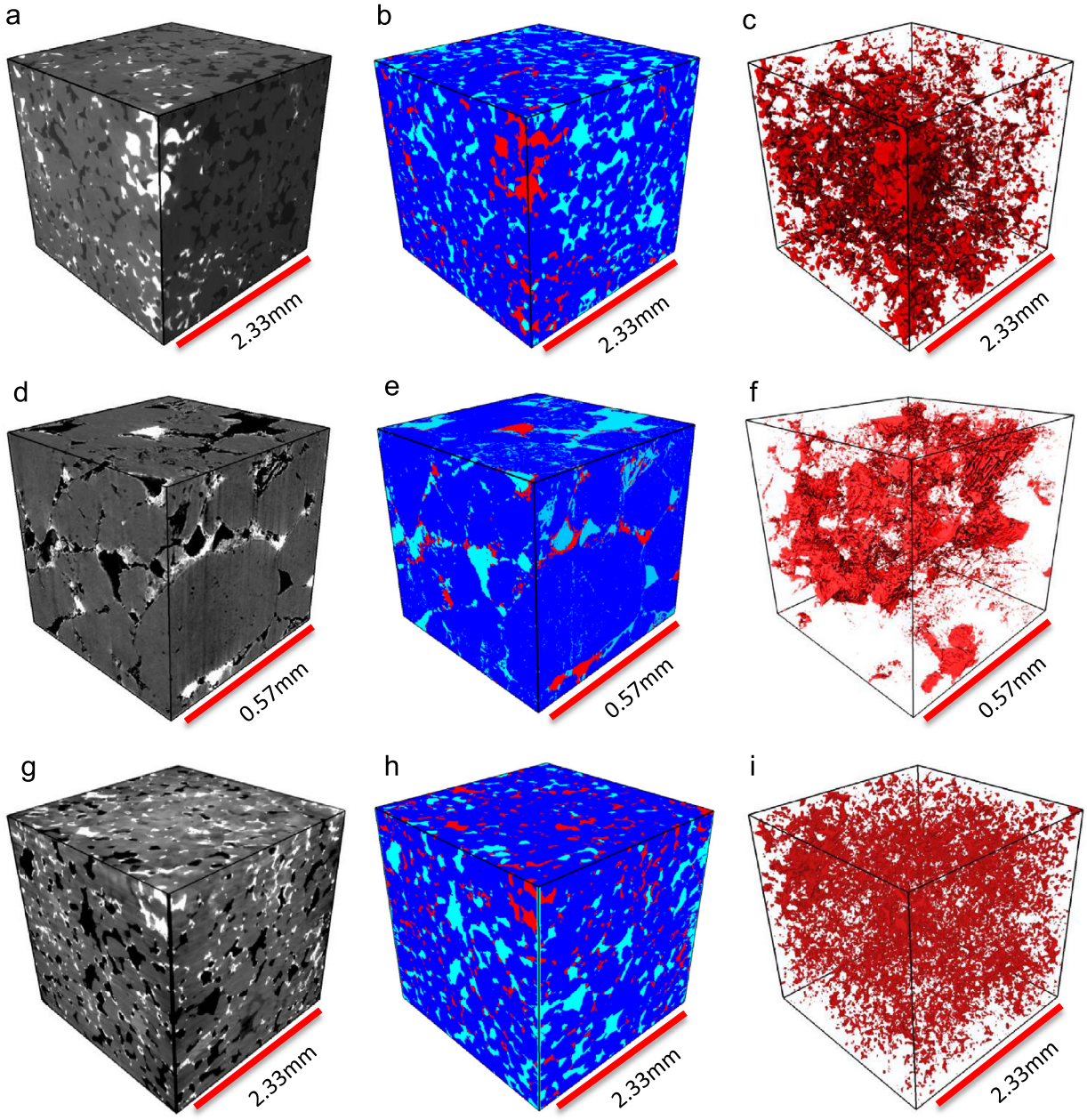

Fig. 11. 3D μCT images of Bentheimer sandstone after formation damage caused by injection of barite suspension. (a) Raw image for sample #1 (10 g barite/L) at 3.4 μm resolution, a cubic volume (12.65 mm^3) is shown, (b) segmented image (a), (c) segmented image for barite (shown in red) only, (d) raw image for sample #1 at a resolution of 0.89 μm, a cubic volume (0.185 mm^3) is shown, (e) segmented image (d), (f) segmented image for barite only, (g) raw image for sample #2 (20 g barite/L) at 3.4 μm resolution, a cubic volume (12.65 mm^3) is shown, (h) segmented image (g), (i) segmented image for barite only at 3.4 μm resolution. In the raw images barite is white, open pore space is black and sandstone is grey; in the segmented images rock is dark blue, barite red and open pore space is light blue. (For interpretation of the references to colour in this figure legend, the reader is referred to the web version of this article.)

smaller relaxation times indicates shrinking pore sizes (Talabi et al., 2009) with the effect more pronounced for the suspension which contained the higher barite concentration.

In addition to a shift of the average T_2 time to shorter times, the T_2 signal distributions shown in Figs. 4 and 5 also clearly show that the longest T_2 peak (associated with the larger pores) decreased

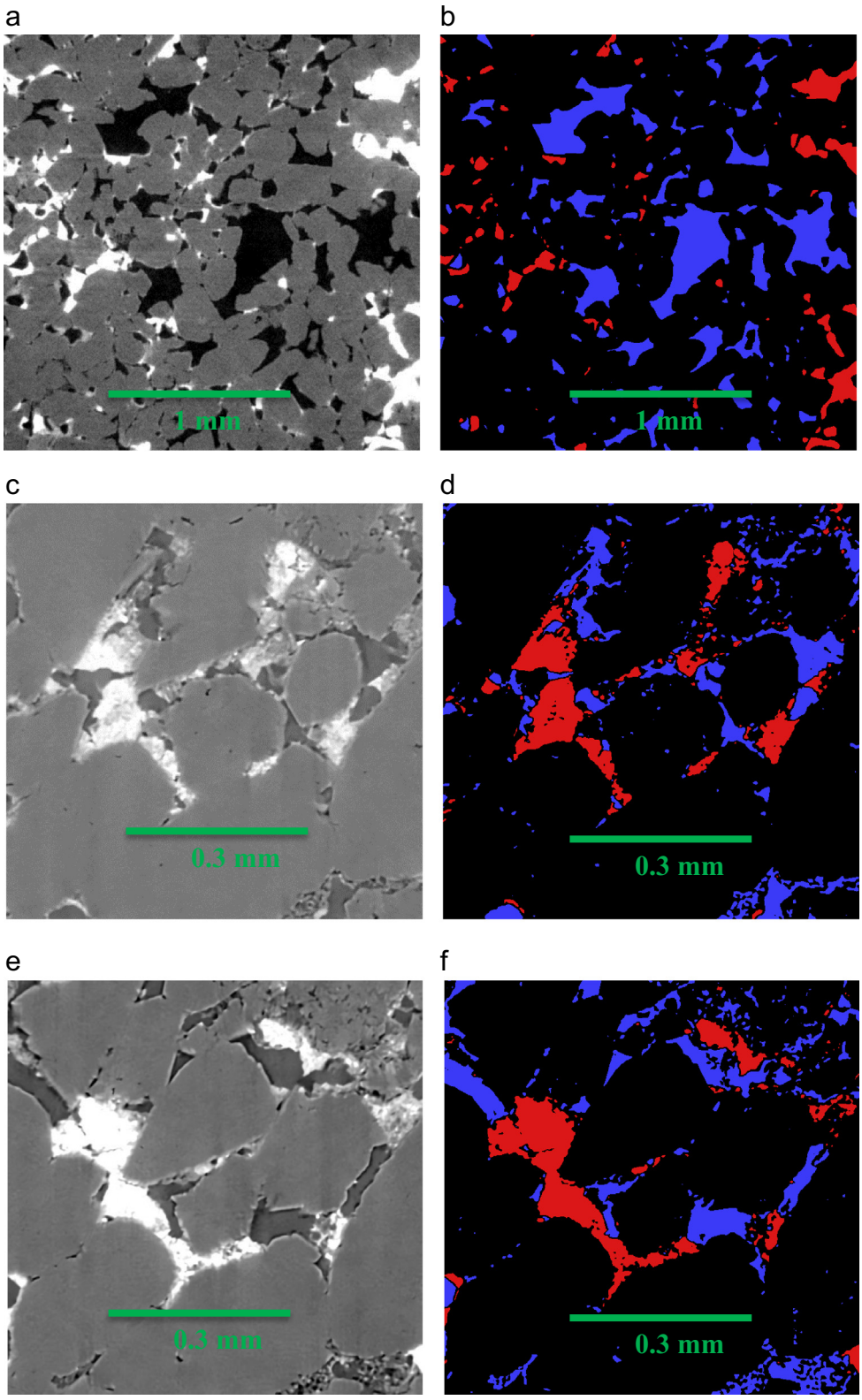

Fig. 12. 2D slices through the rock and pore space: (a) damaged Bentheimer sandstone (sample #2) after injection of particle suspension (20 g/L barite), pores are black/dark grey, sandstone is light grey and barite is white, (b) segmented image, sandstone is black, pore space is blue and barite red at resolutions of 3.4 μm. (c and e) Damaged Bentheimer sandstone (sample #1) after injection of particle suspension (10 g/L barite), pores are dark grey, sandstone is light grey and barite is white, (d and f) segmented images, sandstone is black, pore space is blue and barite red. These images (c–f) show an area of 0.6 mm × 0.67 mm (=0.45 mm^2) at resolutions of 0.89 μm. (For interpretation of the references to colour in this figure legend, the reader is referred to the web version of this article.)

after damage for both samples, with a larger decrease in the long peak for the sample damaged with 20 g/L barite suspension. This indicates that the larger pores in the structure have been plugged and split into smaller pores which is consistent with literature results (Tran et al. 2010); however, Tran et al. (2010)'s NMR results showed smaller changes in porosity (20.6% to 17.6% for their first Berea sample (rock permeability 1240 mD) and 17.5% to 16.9% for their second Berea sample (rock permeability 265 mD)), which was probably caused by the different rock pore morphology and mineralogy and the different particles injected (they used a bentonite/barite mixture, which simulated drilling mud; barite concentration was 5 wt% with 1.2 to 12 μm barite particles sizes).

Consistent with the NMR data, the μCT results showed that particularly large pore sizes (pore diameter >85 μm for sample#1

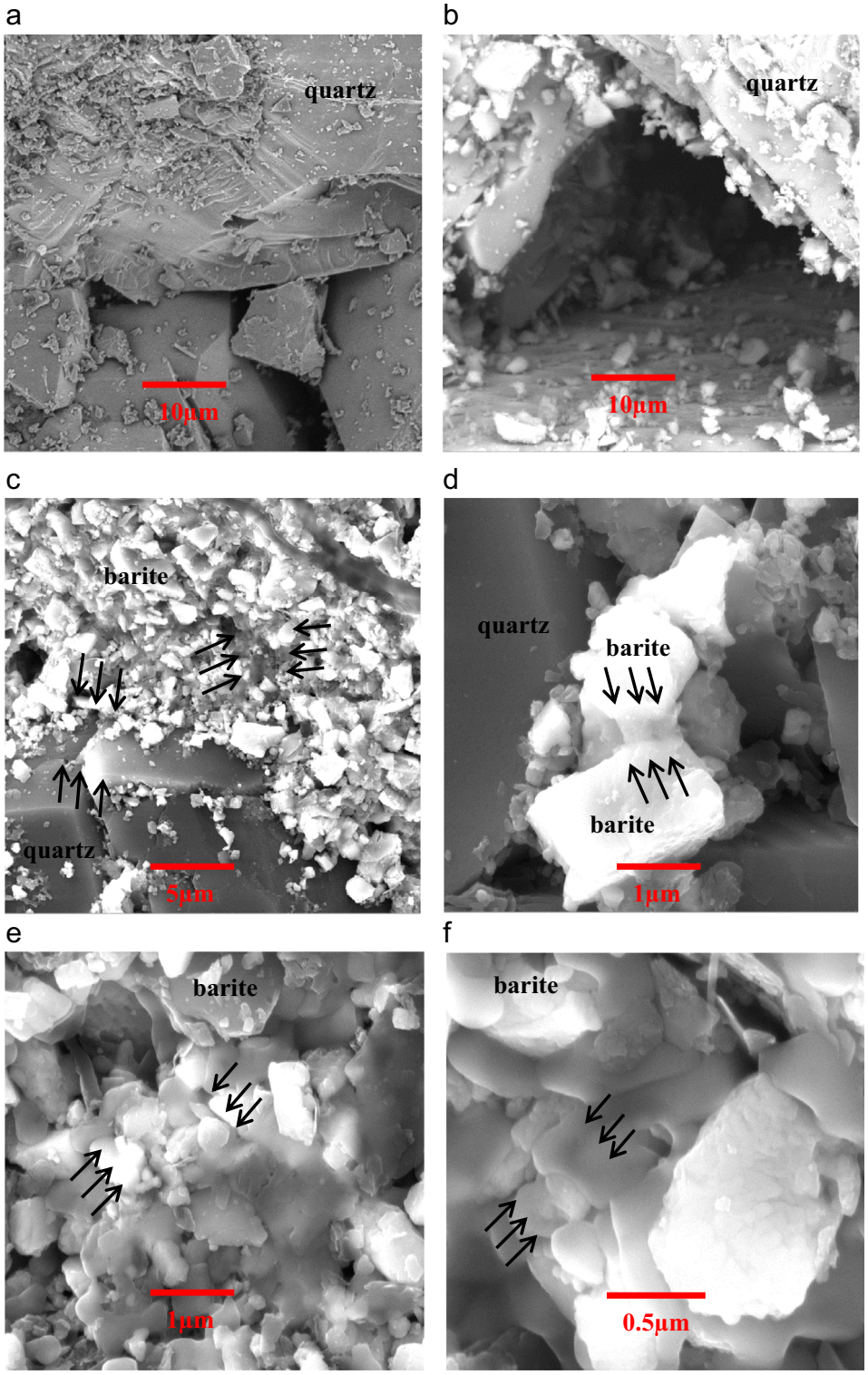

Fig. 13. SEM images of Bentheimer # sample 1 before and after damage (10 g/L barite): (a) and (b) show the undamaged plug, only quartz crystals can be seen, (c) and (d) show the sample after damage, adhesion between quartz (grey) and barite (white) can be seen, (e) and (f) show the adhesion between barite particles in the damaged plug. The black arrows point towards barite–quartz and barite–barite interfaces.

and >136 μm for sample#2) have been damaged, Figs. 6 and 7. Specifically, pores with diameters less than 51 μm (sample#1) and less than 102 μm (sample#2) showed a significantly higher frequency after damage. As mentioned above, the barite particle size distribution comprised sizes from 0.4 to 80 μm and peaked at 25 μm (Fig. 1); while the sandstone pore sizes ranged from ~1 to 340 μm (Figs. 6 and 7). Consequently these distributions overlapped and the fines caused plugging, consistent with predictions based on the aspect ratio β, see discussion below (Civan, 2007; Tran et al., 2009, 2010).

Figs. 8 and 9 show that the amount of barite y (porosity fraction) trapped in the core (a) increased with barite concentration in the suspension, consistent with literature results (Tran et al., 2009,2010) and (b) decreased with depth d following a polynomial $k=0.0202d^2-0.1152d+0.2067$, $R^2=0.81$, (sample#1); $k=0.0345d^2-0.1642d+0.237$, $R^2=0.82$ (sample#2); this is approximately consistent with Nguyen's and Civan's (2005) and Tran et al. (2010)'s results, which showed an exponential reduction. Note that the 10 g barite/L data can also be fitted well with a linear least square fit ($k=-0.046d+0.1558$, $R^2=0.754$); however, a linear fit through the 20 g barite/L data is poor ($k=-0.0256d+0.1958$, $R^2=0.374$).

The reason for this behaviour is visualized in Figs. 10 and 11: the fines flow frequently penetrated into the pore space until a thin pore throat was reached (note that conceptually in pore network models, which quantify the complex pore morphology, pore throats are the smallest pores connecting the larger pore bodies (Dong and Blunt, 2009; Ebrahimi et al., 2013)). We conclude that at these points the fines flow was stopped, i.e. the fines were deposited here first (cp. for instance Fig. 11c, f, and i), and subsequently the larger adjacent pore bodies were filled with barite; this was essentially a jamming process (Civan, 2007). In addition, the fines clustering in Fig. 11c is more localized than in Fig. 11i as a pore throat was just adjacent to the main body of fines agglomerate (right side of cube).

The high resolution images (Fig. 12) provide evidence in terms of the exact plugging mechanism; the water-wet barite particles adhered to the water-wet rock surface, and the barite particles also

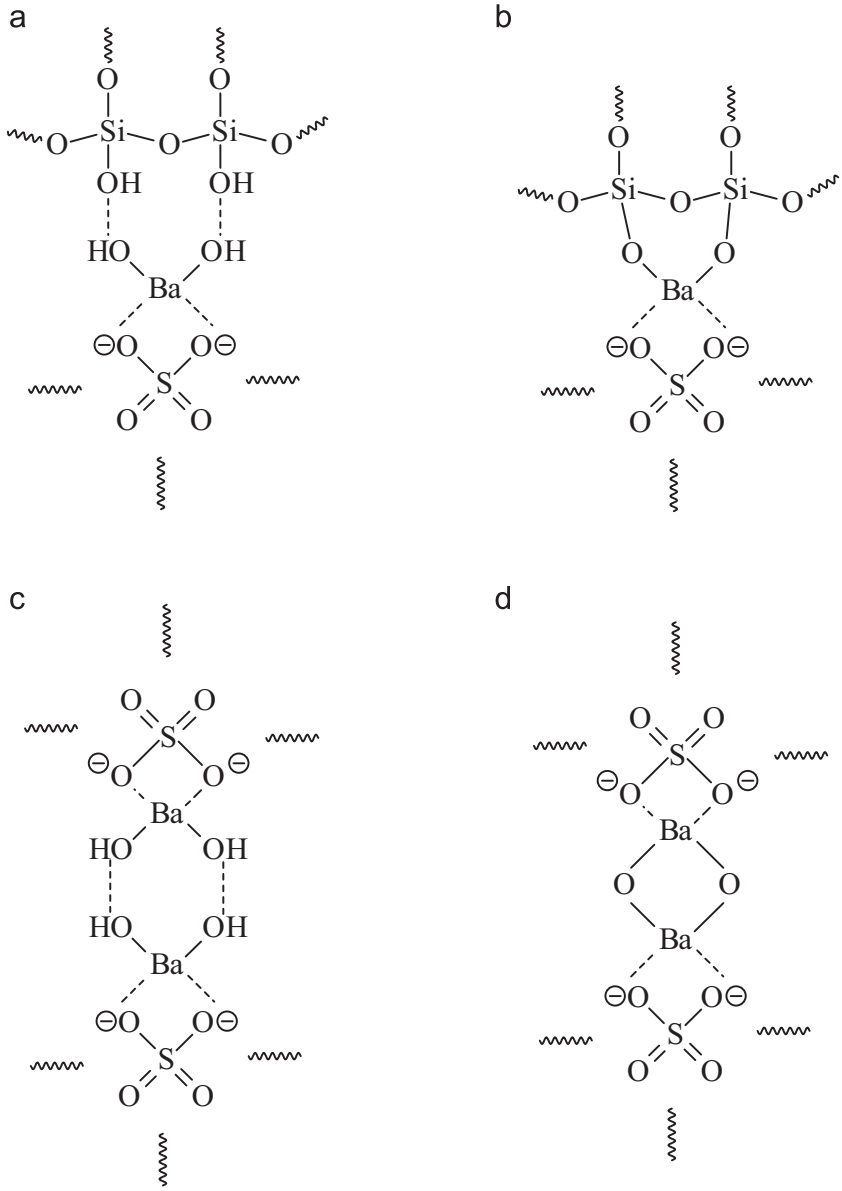

Fig. 14. Barite–barite and quartz–barite surface interactions: the hydroxyl groups attract each other by Debye and Keesom forces or form hydrogen bridges (a) and (c), or a condensation reaction follows where Ba–O–Ba or Si–O–Ba bonds are formed and water is released (b) and (d). These scenarios would trigger tight barite packing and strong adhesion to the sandstone surface.

agglomerated into rather compact conglomerates (Israelachvili, 2011; Torkzaban et al., 2007), which, however, were not loosely packed as previously suggested (Gulati and Maly, 1975; Civan, 2007; Elsaeh and Ramdzani, 2014).

The SEM images shown in Fig. 13c and d also demonstrates that adhesion forces between barite particles and quartz surface were acting; and an analogue situation is illustrated in Fig. 13e and f for the barite–barite particle interactions. Moreover, the SEM images clearly show the arrangement of the particles at the pore-scale. Note that in the SEM images published by Kandarpa and Sparrow (1981), Byrne et al. (2000), Tran et al. (2010), Green et al. (2013), these details were not visible because of low image resolution.

Based on the results discussed above we postulate a new formation damage model which we hypothesize will hold for water-wet fines and water-wet rock (and very likely oil-wet fines and oil-wet rock).

A combination of intermolecular forces and pore geometry leads to the build-up of solid particles in the smallest pore throats. As the pore throats determine permeability (Tiab and Donaldson, 2004) a substantial decrease in permeability is the consequence.

While the impact of pore geometry can be predicted in a straightforward way by using an aspect ratio (β=pore throat to particle diameter length ratio) correlation: if $\beta < 7$, then bridging can occur (Civan, 2007), a prediction of the impact of intermolecular forces is more involved. For the specific system we are considering (i.e. sandstone and barite) we hypothesize that the silanol groups on the quartz (sandstone) surface (Zhuravlev, 2000; McCaughan et al., 2013) strongly attract the hydroxyl groups on the barite surface (Fenter et al., 2001; note that Fenter et al. observed adsorbed water on the barite surface, but could not identify the exact molecular species as the experimental technique they used did not allow them to observe protons), certainly leading to strong Debye and Keesom forces (Israelachvili, 2011), probably hydrogen bridges and possibly condensation reactions (Fig. 14). This scenario would explain the fact that the barite particles were packed tightly as shown in Figs. 12 and 13.

We thus conclude that (a) fines damaging a reservoir might be more difficult to remove than expected based on earlier models, however, (b) chemicals may be found which can break the strong intermolecular bonds and release the fines again. Furthermore we hypothesize that wettability plays a primary role in plugging.

4. Conclusions

We observed formation damage caused by fines injection into sandstone plugs in-situ by μCT and NMR measurements. As expected higher fines concentrations led to greater reduction in porosity and permeability, consistent with the measured production curves and literature data (Krilov et al., 1991; Asghari et al., 1995; Nguyen and Civan, 2005; Tran et al., 2009). The in-situ experiments showed that the amount of fines trapped rapidly decreased with core depth, which confirms earlier measurements (Nguyen and Civan, 2005; Tran et al., 2010); in addition, mainly larger pores were filled with the fines, which was reflected in the shift of the pore size distributions to smaller sizes, this confirms earlier suggestions in the literature (Nguyen and Civan, 2005; Tran et al., 2010). Furthermore, the high resolution μCT images in combination with SEM imaging allowed us to investigate the detailed mechanisms causing the above damage: the barite particles were first trapped in thin pore throats apparently due to the interplay between mechanical and intermolecular forces. Once the throats were plugged, adjacent pore bodies were filled with the fines. Moreover, the barite particles were tightly packed—not loosely as previously suggested (Krilov et al., 1991; Asghari et al., 1995; Nguyen and Civan, 2005; Civan, 2007; Tran et al., 2009), which we hypothesize is due to strong intermolecular forces between the barite particles. These conclusions enabled us to outline a new formation damage model, which we hypothesize will hold for strongly water-wet rock and strongly water-wet fines (and likely in an equivalent way for strongly oil-wet rock and oil-wet fines).

Acknowledgements

The authors thank the National Geosequestration Laboratory (NGL) for providing access to the μCT system VersaXRM-500T (Xradia Ltd). The National Geosequestration Laboratory is a collaboration between Curtin University, CSIRO, and the University of Western Australia established to conduct and deploy critical research and development to enable commercial-scale carbon storage options. Funding for this facility was provided by the Australian Federal Government.

References

Ahmed, T., McKinney, P.D., 2005. Advanced Reservoir Engineering. Gulf Publishing Burlington, USA p. 401 (MA 01803).
Allen, S.G., Stephenson, P.C.L., Strange, J.H., 1997. Morphology of porous media studied by nuclear magnetic resonance. J. Chem. Phys. 106 (18), 7802–7809. http://dx.doi.org/10.1063/1.473780.
Asghari, K., Kharrat, R., Vossoughi, S., 1995. Alteration of permeability by fine particle movement—a water injectivity problem. In: SPE 29006, Presented at the SPE International Symposium on Oilfield Chemistry held in San Antonio, TX, U.S.A., 14–17 February 1995.
Bennion, D.B., Bennion, D.W., Thomas, F.B., Bietz, R.F., 1998. Injection water quality—a key factor to successful waterflooding. Pet. Soc. Can. J. 37 (6), 53–62.
Bennion, D.B., Thomas, F.B., Imer, D., Ma, T., Schulmeister, B., 2011. Water quality considerations resulting in the impaired injectivity of water injection and disposal wells. J. Can. Pet. Technol. 40 (6), 54–61. http://dx.doi.org/10.2118/01-06-05.
Blunt, M.J., Bijeljic, B., Dong, H., Gharbi, O., Iglauer, S., Mostaghimi, P., Pentland, C., 2013. Pore-scale imaging and modelling. Adv. Water Resour. J. 51, 197–216. http://dx.doi.org/10.1016/j.advwatres.2012.03.003 (0).
Bradford, S.A., Torkzaban, S., Simunek, J., 2011. Modeling colloid transport and retention in saturated porous media under unfavorable attachment conditions. Water Resour. Res. 47 (10), W10503. http://dx.doi.org/10.1029/2011WR010812.
Bowers, M.C., Ehrlich, R., Howard, J.J., Kenyon, W.E., 1995. Determination of porosity types from NMR data and their relationship to porosity types derived from thin section. J. Pet. Sci. Eng. 13 (1), 1–14. http://dx.doi.org/10.1016/0920-4105(94)00056-A.
Buades, A., Coll, B., Morel, J.M., 2005. A non-local algorithm for image denoising, presented at the computer vision and pattern recognition. In: Computer Society Conference (CVPR, IEEE), San Diego, CA, 20–25 June 2005.
Byrne, M.T., Patey, I.T.M., Green, J.J., 2007. A new tool for exploration and appraisal—formation damage evaluation. In: SPE 107557-MS. Presented at the European Formation Damage Conference, Scheveningen, The Netherlands, 30 May-1 June 2007.
Byrne, M.T., Spark, I.S.C., Patey, I.T.M., Twynam, A.J., 2000. A laboratory drilling mud overbalance formation damage study utilising cryogenic SEM Techniques. In: SPE 58738, Presented at the SPE International Symposium on Formation Damage Control held in Lafayette, Louisiana, 23–24 February 2000.
Civan, F., 2007. Reservoir Formation Damage Fundamentals, Modeling, Assessment and Mitigation, second ed. Gulf Publishing Company, Houston, USA p. 1114.
Dong, H., Blunt, M.J., 2009. Pore-network extraction from micro-computerized-tomography images. Phys. Rev. E: Stat. Nonlinear Soft Matter Phys. 80 (3), 1–11. http://dx.doi.org/10.1103/PhysRevE.80.036307.
Ebrahimi, N., Jamshidi, A., Iglauer, S., Boozarjomehry, R. B., S., 2013. Genetic algorithm-based pore network extraction from micro-computed tomography images. Chem. Eng. Sci. 92, 157–166 (0).
Elsaeh, A.E., Ramdzani, I.A.B.A., 2014. Pore size and geometry of reservoir rocks used as key factor for drilling and completion fluid design of oil wells. Eur. Sci. J. 10 (10), 102–113.
Fenter, P., McBride, M.T., Srajer, G., Sturchio, N.C., Bosbach, D., 2001. Structure of barite (0 0 1)- and (2 1 0)-water interfaces. J. Phys. Chem. 105 (34), 8112–8119. http://dx.doi.org/10.1021/jp0105600.
Fischer, S., Zemke, K., Liebscher, A., Wandrey, M., 2011. Petrophysical and petrochemical effects of long-term CO_2-exposure experiments on brine-saturated reservoir sandstone. Energy Procedia 4 (0), 4487–4494.
Fridjonsson, E.O., Hasan, A.B., Fourie, A.B., Johns, M.L., 2013. Pore structure in a gold mine cemented paste backfill. Miner. Eng. J. 53, 144–151.
Green, J., Cameron, R., Patey, I., Nagassar, V., Quine, M., 2013. Use of micro-CT scanning visualisations to improve interpretation of formation damage laboratory tests including a case study from the South Morecambe Field. In: SPE 165110, Presented at the SPE European Formation Damage Conference, Noordwijk, The Netherlands, 5-7 June 2013.

Gulati, M.S., Maly, G.P., 1975. Thin-section and permeability studies call for smaller gravels in gravel packing. J. Pet. Technol. 27 (1), 107–112. http://dx.doi.org/10.2118/4773-PA.
Hidajat, I., Rastogi, A., Singh, M., Mohanty, K.K., 2002. Transport properties of porous media reconstructed from thin-sections. Soc. Pet. Eng. J. 7 (1), 40–48. http://dx.doi.org/10.2118/77270-PA.
Iglauer, S., Favretto, S., Spinelli, G., Schena, G., Blunt, M.J., 2010. X-ray tomography measurements of power-law cluster size distributions for the nonwetting phase in sandstones. Phys. Rev. E: Stat. Nonlinear Soft Matter Phys. 82, 05631.
Israelachvili, J.N., 2011. Intermolecular and Surface Forces, third ed. Academic Press, London p. 667.
Kandarpa, V., Sparrow, J.T., 1981. A useful technique to study particle invasion in porous media by backscattered electron imaging. In: SPE 10134, Presented at the SPE 56th Annual Fall Technical Conference and Exhibition, San Antonio, Texas, October 5-7, 1981.
Kleinberg, R.L., Kenyon, W.E., Mitra, P.P., 1994. Mechanism of NMR relaxation of fluids in rock. J. Magn. Reson. Ser. 108, 206–214.
Krilov, Z., Steiner, I., Goricnik, B., Wojtanowicz, A.J., Cabrajac, S., 1991. Quantitative determination of solids invasion and formation damage using CAT scan and barite suspensions. In: SPE 23102, Presented at the SPE Offshore Europe Conference, UK, Aberdeen, 3-6 September 1991.
Krueger, R.G., 1967. Effect of pressure drawdown on clean-up of clay- or silt-blocked sandstone. Soc. Pet. Eng. J. 19 (3), 397–403. http://dx.doi.org/10.2118/1605-PApp , http://dx.doi.org/10.2118/1605-PA.
Liaw, H.K., Kulkarni, R., Chen, S., Watson, A.T., 1996. Characterization of fluid distributions in porous media by NMR techniques. AIChE J. 42 (2), 538–546.
Mahmoudi, H., Spahis, N., Goosen, M.F., Ghaffour, N., Drouiche, N., Ouagued, A., 2010. Application of geothermal energy for heating and fresh water production in a brackish water greenhouse desalination unit: a case study from Algeria. Renewable Sustainable Energy Rev. 14 (1), 512–517.
McCaughan, J., Iglauer, S., Bresme, F., 2013. Molecular dynamics simulation of water/CO_2-quartz interfacial properties: application to subsurface gas injection. Energy Procedia J. 37, 5387–5402. http://dx.doi.org/10.1016/j.egypro.2013.06.457 (0).
McDowell-Boyer, L.M., Hunt, J.R., Sitar, N., 1986. Particle transport through porous media. Water Resources Res. 22 (13), 1901–1921. http://dx.doi.org/10.1029/WR022i013p01901.
Nguyen, V., Civan, F., 2005. Modeling particle migration and deposition in porous media by parallel pathways with exchange. Chapter 11. In: Vafai, K. (Ed.), Handbook of Porous Media, second ed. CRC Press, Taylor and Francis Group, Boca Raton, FL, pp. 457–484.
Nowak, T.J., Krueger, R.F., 1951. The effect of mud filtrates and mud particles upon the permeabilities of cores. In: American Petroleum Institute (API-51-164). Presented at Drilling and Production Practice Conference (New York, New York, 1 January 1951).
Okabe, H., Tsuchiya, Y., Pentland, C.H., Iglauer, S., M.J. Blunt, 2013. Residual CO_2 saturation distributions in rock samples measured by X-ray CT. In: Advances in X-ray Tomography, chapter 45, pp. 381–389 (Ed., K Lui).
Otsu, N., 1979. A threshold selection method from gray-level histograms. IEEE Trans. Syst. Man. Cyber 9 (10), 62–66.
Potter, D.K., Al-Ghamdi, T.M., Ivakhnenko, O.P., 2011. Sensitive Carbonate Reservoir Rock Characterization From Magnetic Hysteresis Curves and Correlation with Petrophysical Properties. Petrophysics 52 (1), 50–57.
Rosenbrand, E., Kjøller, C., Riis, J.F., Kets, F., Fabricius, I.L., 2015. Different effects of temperature and salinity on permeability reduction by fines migration in Berea sandstone. Geothermics 53, 225–235. http://dx.doi.org/10.1016/j.geothermics.2014.06.004 (0).
Rosenbrand, E., Haugwitz, C., Jacobsen, P.S.M., Kjøller, C., Fabricius, I.L., 2014. The effect of hot water injection on sandstone permeability. Geothermics 50 (0), 155–166. http://dx.doi.org/10.1016/j.geothermics.2013.09.006.
Ryan, J.N., Elimelech, M., 1996. Colloid mobilization and transport in groundwater. Colloids and Surfaces 107, 1–56.
Seright, R.S., Prodanovic, M., Lindquist, W.B., 2006. X-ray computed microtomography studies of fluid partitioning in drainage and imbibition before and after gel placement: disproportionate permeability reduction. Soc. Pet. Eng. J. 11 (2), 159–170. http://dx.doi.org/10.2118/89393-PA.
Talabi, O., AlSayari, S., Iglauer, S., Blunt, M.J., 2009. Pore-scale simulation of NMR response. J. Pet. Sci. Eng. 67 (3–4), 168–178. http://dx.doi.org/10.1016/j.petrol.2009.05.013.
Tiab, D., Donaldson, E.C., 2004. Petrophysics—Theory and Practice of Measuring Reservoir Rock and Fluid Transport Properties, second ed. Gulf Publishing Co., Elsevier, USA p. 889.
Tran, T.V., Civan, F., Robb, I.D., 2009. Correlating flowing time and condition for perforation plugging by suspended particles. Soc. Pet. Eng. J. 24 (3), 398–403. http://dx.doi.org/10.2118/120847-PA.
Tran, T.V., Civan, F., Robb, I.D., 2010. Effect of permeability impairment by suspended particles on invasion of drilling fluids. In: IADC/SPE 133724, Presented at the IADC/SPE Asia Pacific Drilling Technology Conference and Exhibition, Vietnam, Ho Chi Minh, 1–3 November 2010.
Torkzaban, S., Bradford, S.A., Walker, S.L., 2007. Resolving the coupled effects of hydrodynamics and DLVO forces on colloid attachment in porous media. Langmuir 23 (19), 9652–9660. http://dx.doi.org/10.1021/la700995e.
Wildenschild, D., Sheppard, A.P., 2013. X-ray imaging and analysis techniques for quantifying pore-scale structure and processes in subsurface porous medium systems. Adv. Water Resour. 51 (0), 217–246.
Zhuravlev, L.T., 2000. The surface chemistry of amorphous silica. Zhuravlev model. Colloids Surf. A Physicochem. Eng. Aspects 173 (1–3), 1–38.